

# Loops Mediate Agonist-Induced Activation of the Stimulator of Interferon Genes Protein

Rui Li, Lin Chen, Xinheng He, Duanhua Cao, Zehong Zhang, Hualiang Jiang,\* Kaixian Chen,\* and Xi Cheng\*



Cite This: <https://doi.org/10.1021/acs.jcim.3c00984>



Read Online

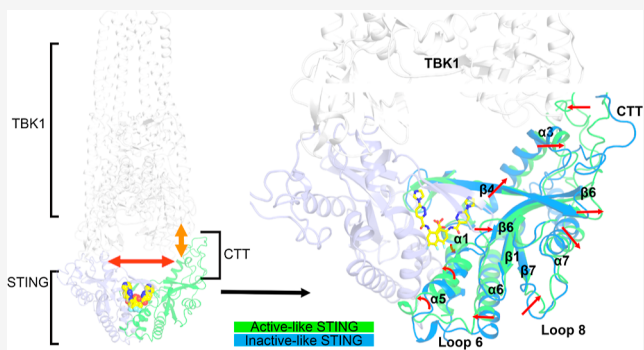
ACCESS |

Metrics & More

Article Recommendations

Supporting Information

**ABSTRACT:** The stimulator of interferon genes (STING) is an important therapeutic target for cancer diseases. The activated STING recruits downstream tank-binding kinase 1 (TBK1) to trigger several important immune responses. However, the molecular mechanism of how agonist molecules mediate the STING–TBK1 interactions remains elusive. Here, we performed molecular dynamics simulations to capture the conformational changes of STING and TBK1 upon agonist binding. Our simulations revealed that multiple helices ( $\alpha 5$ – $\alpha 7$ ) and especially three loops (loop 6, loop 8, and C-terminal tail) of STING participated in the allosteric mediation of the STING–TBK1 interactions. Consistent results were also observed in the simulations of the constitutive activating mutant of STING (R284S). We further identified  $\alpha 5$  as a key region in this agonist-induced activation mechanism of STING. Free-energy perturbation calculations of multiple STING agonists demonstrated that an alkynyl group targeting  $\alpha 5$  is a determinant for agonist activities. These results not only offer deeper insights into the agonist-induced allosteric mediation of STING–TBK1 interactions but also provide a guidance for future drug development of this important therapeutic target.



## INTRODUCTION

The stimulator of interferon genes (STING) protein plays a crucial role in several innate immune and biological processes, including antitumor immunity and maintenance of microbiome homeostasis.<sup>1–12</sup> Upon cyclic GMP-AMP (cGAMP) binding, STING is phosphorylated by tank-binding kinase 1 (TBK1) to initiate the activation of the type-I interferon pathway.<sup>13–16</sup> Activation of the STING protein subsequently results in the release of chemokines and cytokines.<sup>17,18</sup> The development of STING agonists is therefore being pursued as a promising strategy for cancer therapy.

As an endogenous agonist of STING, cGAMP binds to a dimeric interface, termed cyclic dinucleotide-binding domain (CBD).<sup>19</sup> Various agonists, including the non-nucleotide ligand SR-717, have been reported to bind to the CBD to activate STING.<sup>20–24</sup> The CBD consists of three helices ( $\alpha 1$ ,  $\alpha 2$ , and  $\alpha 5$ ) and four strands ( $\beta 2$ ,  $\beta 3$ ,  $\beta 4$ , and  $\beta 6$ ) (Figure S1). Researchers have identified the  $\beta 4$  residue R238 as an essential agonist binding residue within the STING complex.<sup>25–28</sup> According to the crystal structure analysis of the agonist-bound STING complex, agonist binding causes conformational changes in the CBD, including the movement of the  $\alpha 2$  helix.<sup>19,21,23,29</sup> Such agonist-induced conformations of the CBD have been suggested to be associated with “active-like” states of STING.<sup>28–31</sup> However, the CBD is located in the

center of the STING, which is far away from the protein-binding interface of STING. In fact, the distance between CBD (such as  $\alpha 5$ ) and the TBK1-binding interface is more than 20 Å.<sup>29</sup> It remains largely unknown how agonists allosterically activate STING and subsequently recruit TBK1. The complex structure model including all these elements is still missing.

In this study, we performed molecular dynamics (MD) simulations to investigate the mechanism of agonist-induced activation in the STING–TBK1 binding process. We also simulated a disease-associated constitutive activating mutant (R284S) of STING to investigate the STING–TBK1 interactions without an agonist. Further, based on our simulation results, we performed relative binding free-energy calculations for seven STING agonists (including SR-717) to offer insights for future drug development of this important target for cancer immunotherapy.

Received: June 30, 2023

Published: October 13, 2023

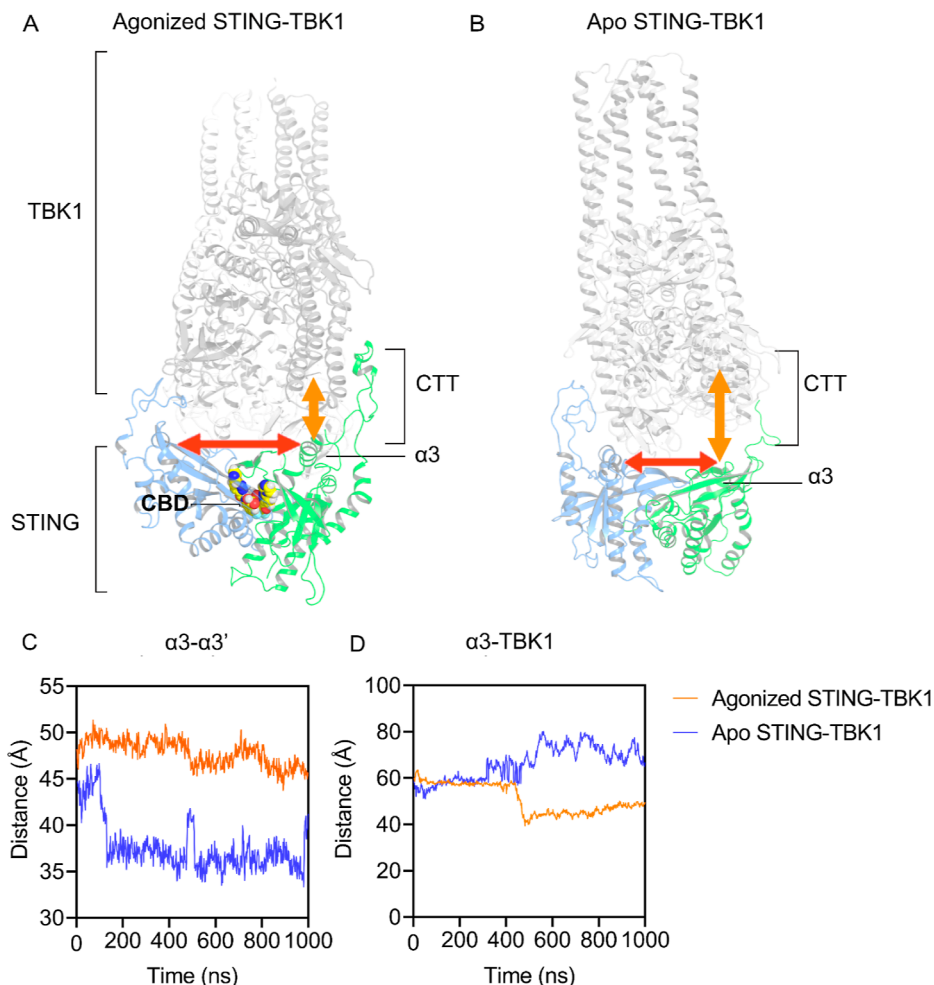


**Figure 1.** MD simulations of STING–TBK1 complexes with and without agonists. (A,B) Representative simulation snapshots of the agonized-STING–TBK1 and apo STING–TBK1 systems. The movement of N-terminal regions of  $\alpha 3$  and  $\alpha 3'$  of STING is indicated with red arrows. The movement of  $\alpha 3$  away from TBK1 is indicated by orange arrows. (C)  $C\alpha$  distance between the N-terminal regions of  $\alpha 3$  and  $\alpha 3'$  as a function of time in the agonized-STING–TBK1 and apo STING–TBK1 simulations. (D)  $C\alpha$  distance between  $\alpha 3$  and TBK1 as a function of time in the agonized-STING–TBK1 and apo STING–TBK1 simulations.

## RESULTS AND DISCUSSION

**Agonist Stabilizes the STING–TBK1 Interactions.** We performed 1000 ns MD simulations of STING–TBK1 complexes with and without agonist SR-717, termed agonized-STING–TBK1 and apo STING–TBK1 systems, respectively (Figures 1A,B and S2). Upon agonist binding, the average distances between subunit  $\alpha 3$  helices of STING increased to  $46.16 \pm 0.90$  Å, while it was  $36.61 \pm 1.57$  Å in the apo STING–TBK1 system (Figures 1C and S3A and Table S1). Notably, STING started to dissociate with the TBK1 in the apo STING–TBK1 system. The distance between the  $\alpha 3$  helix of STING and TBK1 increased to  $70.09 \pm 2.93$  Å in the apo STING–TBK1 system, while that distance was  $47.76 \pm 1.29$  Å in the agonized-STING–TBK1 system (Figures 1D and S3B and Table S1). Moreover, the TBK1-binding interface of one C-terminal tail (CTT) of STING reduced to  $517.30 \pm 61.19$  Å<sup>2</sup> in the apo STING–TBK1 system, which was significantly smaller than that in the agonized-STING–TBK1 system ( $1197.00 \pm 263.00$  Å<sup>2</sup>). These findings suggested that the agonist SR-717 facilitated the interactions between STING and TBK1.

Our MD simulations showed that the agonist SR-717 mediates the movement of  $\alpha 3$  by binding to  $\beta 4$ ,  $\beta 6$ , and  $\alpha 1$

(Figure 2). In the agonized-STING–TBK1 system, the insertion of the imidazole group of SR-717 pushed away the  $\alpha 3$  of STING toward TBK1 by disrupting the hydrogen bonding between  $\beta 4$  residue N242 and  $\alpha 3$  residue R178 (Figure 3A). The average heavy atom distance between R178 and N242 was  $7.91 \pm 0.87$  Å in the agonized-STING–TBK1 system, which was significantly longer than that in the apo STING–TBK1 system ( $3.02 \pm 0.22$  Å) (Figures S4 and S5 and Table S1). Meanwhile,  $\beta 6$  moved away from  $\alpha 1$  to stabilize  $\alpha 3$  in the agonized-STING–TBK1 system (Figure 2). In particular, the  $\alpha 1$  residue Y163 formed a hydrogen bond with the backbone oxygen of the  $\beta 6$  residue Y261 with a heavy atom distance of  $2.79 \pm 0.18$  Å in the apo system, while it was  $4.43 \pm 0.32$  Å in the agonized system (Figures 3B, S4, and S5 and Table S1).  $\beta 6$  also stabilized  $\alpha 3$  in the agonized-STING–TBK1 system (Figure 2). The R253 of  $\beta 6$  made stable contact with the L190 of  $\alpha 3$  (with the average heavy atom distance of  $4.82 \pm 1.02$  Å) in the agonized-STING–TBK1 system, while the distance between these two residues was  $4.78 \pm 0.86$  Å in the apo system (Figures 3C, S4, and S5 and Table S1).

On the other hand, the agonist SR-717 could also modulate the remote protein–protein interface between STING and TBK1 via several loops, including loop 6, loop 8, and CTT

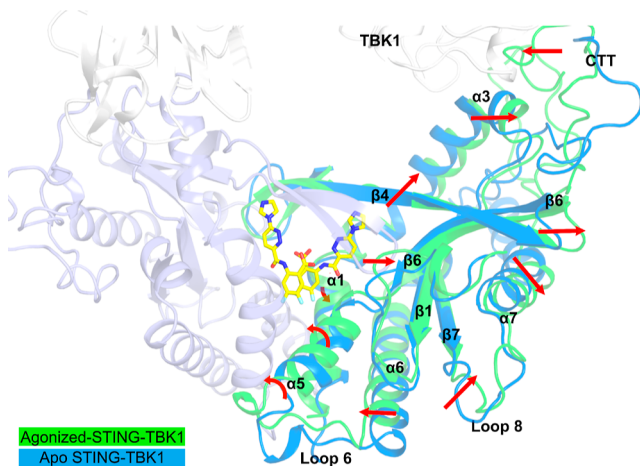


**Figure 2.** Representative simulation models showing the allosteric pathways of agonist-induced activation of STING. The agonist SR-717 is colored yellow, and TBK1 is colored white. A chain of STING is colored in green (for the agonized-STING–TBK1 system) and blue (for the apo STING–TBK1 system), and the other is colored in white-blue. The allosteric pathways are indicated with red arrows.

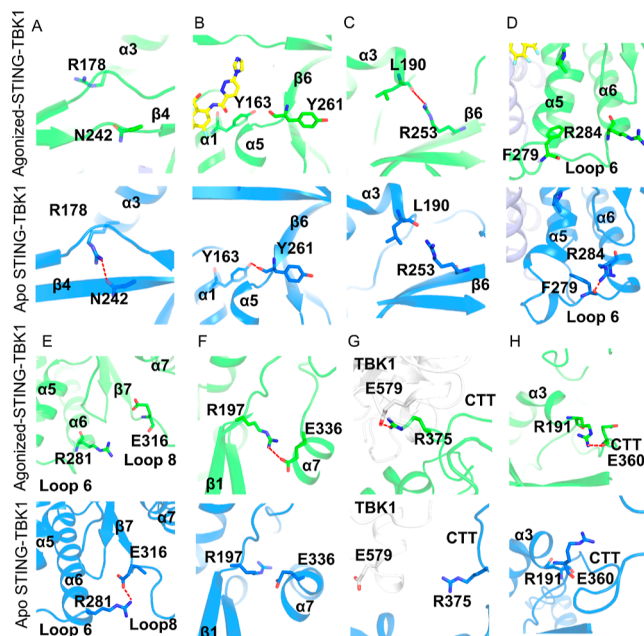


**Figure 3.** Key interactions in the agonized-induced activation of STING in simulations. (A–H) Key residues of  $\alpha 3$  and  $\beta 4$  (A),  $\alpha 1$  and  $\beta 6$  (B),  $\alpha 3$  and  $\beta 6$  (C), loop 6 and  $\alpha 6$  (D),  $\alpha 6$  and loop 8 (E),  $\beta 1$  and  $\alpha 7$  (F), CTT and TBK1 (G), and CTT and  $\alpha 3$  (H) in the agonized-STING–TBK1 (green) and apo STING–TBK1 (blue) systems. The key residues and agonist SR-717 are shown as sticks. Putative hydrogen bonds and salt bridges are shown as red dashed lines.

(Figure 2). In the agonized-STING–TBK1 system, SR-717 rotated the  $\alpha 5$  helix and dragged the  $\alpha 6$  helix away from loop 8 through loop 6, resulting in the movement of  $\alpha 7$  and CTT (Figure 2). The insertion of the fluorine group of the agonist disrupted the interaction between F279 in loop 6 and R284 of  $\alpha 6$  (Figure 3D). The average heavy atom distance between R284 and F279 was  $3.43 \pm 0.76$  Å in the apo STING–TBK1 system, while that increased to  $4.78 \pm 0.55$  Å in the agonized one (Figures S4 and S5 and Table S1). Then, E316 of loop 8 dissociated with R281 of  $\alpha 6$  in the agonized system. R281 and

E316 could form a salt bridge in the apo STING–TBK1 system, but that distance between them increased to  $15.10 \pm 3.95$  Å in the agonized system (Figures 3E, S4, and S5 and Table S1). Linked to loop 8, the  $\alpha 7$  helix moved against  $\beta 1$  (Figure 2). The  $\alpha 7$  residue E336 could interact with the  $\beta 1$  residue R197 in the agonized-STING–TBK1 system (Figure 3F). The average heavy atom distance between E336 and R197 was  $3.68 \pm 1.06$  Å in the agonized-STING–TBK1 system, while that increased to  $5.28 \pm 0.30$  Å in the apo system (Figures S4 and S5 and Table S1). Connected to  $\alpha 7$ , the CTT moved along with  $\alpha 7$  to interact with TBK1 (Figure 2). In the agonized-STING–TBK1 system, R375 of CTT and E579 of TBK1 had an average heavy atom distance of  $4.40 \pm 0.89$  Å in the agonized system, while that distance increased to  $17.82 \pm 2.64$  Å in the apo system (Figures 3G, S4 and S5 and Table S1). The main probability of this distance distribution of agonized-STING–TBK1 was located around 3 Å (Figures S4). In addition, CTT could further stabilize  $\alpha 3$  in the agonized system (Figures 2 and 3H). The average heavy atom distance between the  $\alpha 3$  residue R191 and the CTT residue E360 was  $3.77 \pm 1.31$  Å in the agonized-STING–TBK1 system, while that was  $10.01 \pm 1.37$  Å in the apo system (Figures S4 and S5 and Table S1).

Collectively, the agonist molecule SR-717 could allosterically modulate STING in two ways (Figure 2). One involves  $\beta 4$  and  $\beta 6$  to make an “active-like” conformation of STING by increasing the intersubunit  $\alpha 3$  distance; the other includes multiple helices ( $\alpha 1$ ,  $\alpha 5$ ,  $\alpha 6$ , and  $\alpha 7$ ) and loops (loop 6, loop 8, and CTT), to enhance the direct interactions between STING and TBK1. In a previous structure–function analysis of STING, Gao et al. reported the distance between  $\alpha 3$  helices significantly increased upon binding of an agonist c[G(2',S')-pA(3',S')p],<sup>19</sup> highly consistent with our simulation results. Moreover, the corresponding distances between  $\alpha 3$  helices in the experimental structures of agonist-bound STING range from 40.2 to 63.2 Å (Table S2), agreeing with our models. On the other hand, previous mass spectrometry and functional assays had showed the CTT of STING was phosphorylated by TBK1 and determined the recruitment of TBK1.<sup>32,33</sup> In the binding study of human STING and TBK1, the mutation of a CTT residue R375 reduced the binding affinity by 30-fold.<sup>33</sup> In addition, the R375A mutation reduced the phosphorylation of TBK1, STING, and IRF-3.<sup>33</sup> Corresponding to the R375 of human STING, the R374 has also been reported to determine the activity of mouse STING.<sup>32</sup> Compared with the wild-type mouse STING, the R374A mutant showed a significant decrease in activation activity. These experimental data are consistent with our simulation observation that the CTT residue R375 interacted with the TBK1 (Figure 3G). Our simulation study proposed a possible molecular model to understand how agonists could allosterically mediate CTT to interact with TBK1 via these important helices and loops.

**Constitutive Activating Mutation R284S Stabilizes the Interactions between STING and TBK1.** We also performed MD simulations for a disease-associated constitutive activating mutant of STING, termed apo R284S-TBK1 (Figure 4A). In our MD simulations, the mutation R284S of the  $\alpha 6$  helix mediated multiple loops, including loop 6, loop 8, and CTT of STING, that interact with TBK1 (Figure 4B), similar to the remote allosteric modulation of the agonized-STING–TBK1 system (Figure 2). Substituting the arginine of the  $\alpha 6$  with a small polar residue, i.e., serine, disrupted its interaction with loop 6 (Figure 5A). The average heavy atom distance

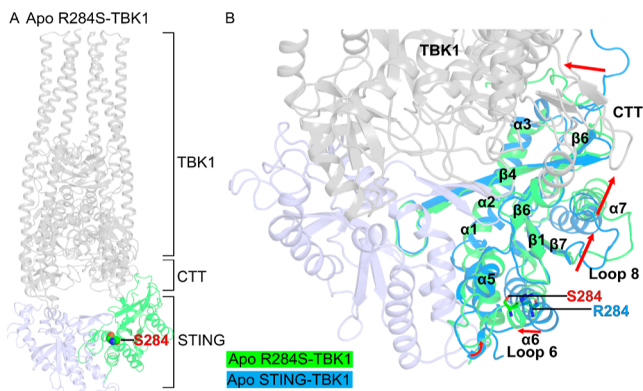


**Figure 4.** MD simulations involve a mutant R284S of STING. (A) Representative simulation snapshot of the apo R284S-TBK1 system. (B) Representative simulation models showing the allosteric pathway of mutation-induced activation of STING. The TBK1 is colored white. A chain of STING is colored green (for the apo R284S-TBK1 system) and blue (for the apo STING-TBK1 system), and the other is colored white-blue. The allosteric pathway is indicated with red arrows.

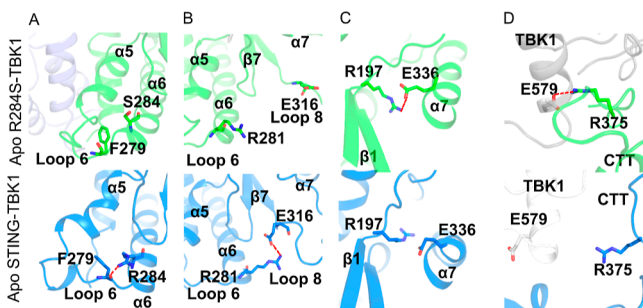


**Figure 5.** Key interactions in the mutation-induced activation of STING in simulations. (A–D) Key residues of loop 6 and  $\alpha$ 6 (A),  $\alpha$ 6 and loop 8 (B),  $\beta$ 1 and  $\alpha$ 7 (C), and CTT and TBK1 (D) in the apo R284S-TBK1 (green) and apo STING-TBK1 (blue) systems. The key residues are shown as sticks. Putative hydrogen bonds and salt bridges are shown as red dashed lines.

between  $\alpha$ 6 residue S284 and loop 6 residue F279 increased to  $6.44 \pm 0.40$  Å in the apo R284S-TBK1 system (Figures S4 and S5 and Table S1). Consequently, in the R284S mutant system, loop 6 and loop 8 dissociated with each other (Figure 4B), and the average heavy atom distance between the loop 6 residue R281 and loop 8 residue E316 increased to  $15.70 \pm 1.87$  Å (Figure 5B, S4 and S5 and Table S1). Linked to loop 8,  $\alpha$ 7 moved along with  $\beta$ 1 and determined the arrangement of CTT (Figure 4B). In the apo R284S-TBK1 system, the  $\alpha$ 7 residue E336 formed a salt bridge with the  $\beta$ 1 residue R197 with an average heavy atom distance of  $3.12 \pm 0.57$  Å (Figures 5C, S4 and S5 and Table S1). Eventually, the impact of mutation was transmitted to CTT, resulting in the interaction of CTT and TBK1 (Figure 4B). The side chain of CTT residue R375 stably interacted with the side chain of the TBK1 residue E579 with the average heavy atom distance of  $3.72 \pm 0.92$  Å in the apo R284S-TBK1 system (Figures 5D, S4 and S5 and Table S1). Consistently, the TBK1-binding interface of one CTT of STING was  $937.5 \pm 43.8$  Å. Compared with the apo STING-TBK1 system,  $\alpha$ 5,  $\alpha$ 6,  $\alpha$ 7, loop 6, loop 8, and CTT of R284S had secondary structures similar to those in the agonized-TBK1 system (Figure 4). In particular, the “active-like” STING had reduced the helix scores of  $\alpha$ 5 and  $\alpha$ 7 and increased the

helix scores of  $\alpha$ 6, loop 6, and loop 8 (Figure S6). All of these results suggested that the R284S had a similar “active-like” conformation as the agonized STING (Figures 2 and S6 and S7).

Linked to loop 6, helix  $\alpha$ 5 also rotated to mediate helix  $\alpha$ 3 in the apo R284S-TBK1 system. Similar to the agonized-STING-TBK1 system,  $\alpha$ 1,  $\beta$ 4, and  $\beta$ 6 participated in the allosteric modulation in the mutant system (Figure 4B). In particular, the average heavy atom distance between  $\alpha$ 1 residue Y163 and  $\beta$ 6 residue Y261 increased to  $4.46 \pm 0.53$  Å, and the distance between  $\alpha$ 3 residue R178 and  $\beta$ 4 residue N242 of the apo R284S-TBK1 complex increased to  $11.97 \pm 0.77$  Å in the apo R284S-TBK1 system (Figures S4, S5, S8 and Table S1). In the mutant system, the distance between different  $\alpha$ 3 subunits of the mutation complex was  $44.63 \pm 1.15$  Å, which was shorter than that of the agonized system ( $46.16 \pm 0.90$  Å) but longer than that of the apo system ( $36.61 \pm 1.57$  Å; Table S1). The distance between the R284S mutation site and the  $\alpha$ 3 helix was about two folds of that between the helix and the agonist-binding site. The longer distance might lead to the reduced effect of the mutation on mediating the  $\alpha$ 3 helix.

Together, the influence of the agonist SR-717 or the mutation R284S could be transmitted through  $\alpha$ 5, loop 6, loop 8, and CTT to the STING-TBK1 interface, highlighting their importance in the activation of STING. Our findings not only provide possible structural models for understanding the activation mechanism of STING and TBK1 but also could be employed in the assessment of STING agonists.

**Simulation-Based Bioactive Analysis of STING Agonists.** Molecular Mechanics Poisson–Boltzmann Surface Area (MMPSA) has been broadly applied to model molecular recognition for drug discovery and lead optimization.<sup>34</sup> We used the MMPSA binding free-energy calculation to quantitatively characterize SR-717 binding in our simulations. The total binding energy of the SR-717 and STING was  $-56.786$  kcal/mol (Table S3). Eight residues of  $\alpha$ 1,  $\beta$ 4, and  $\alpha$ 5 bound to SR-717 with a total binding energy of less than  $-1.0$  kcal/mol (Figure 6). Residues of  $\beta$ 4,  $\alpha$ 1, and  $\alpha$ 5 made major contributions to agonist binding with a total binding energy of less than  $-2.0$  kcal/mol (Figure 6B).

Integrating with our MD simulation results, we conducted free-energy perturbation (FEP) calculations to decipher the structure–function relationship of seven STING agonists.<sup>35</sup> Compared with the ligand-binding free energy of SR-717 to

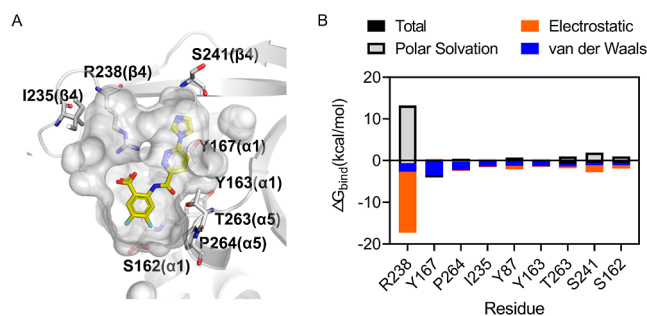


**Figure 6.** Binding model of SR-717 to STING. (A) Representative simulation model showing the key residues of STING binding to SR-717. Key residues and SR-717 (yellow) are depicted as sticks. The agonist-binding pocket is shown as the surface. (B) Decomposition of the total binding free energies ( $\Delta G_{\text{bind}}$ ) on a per-residue basis in the agonized-STING complex.

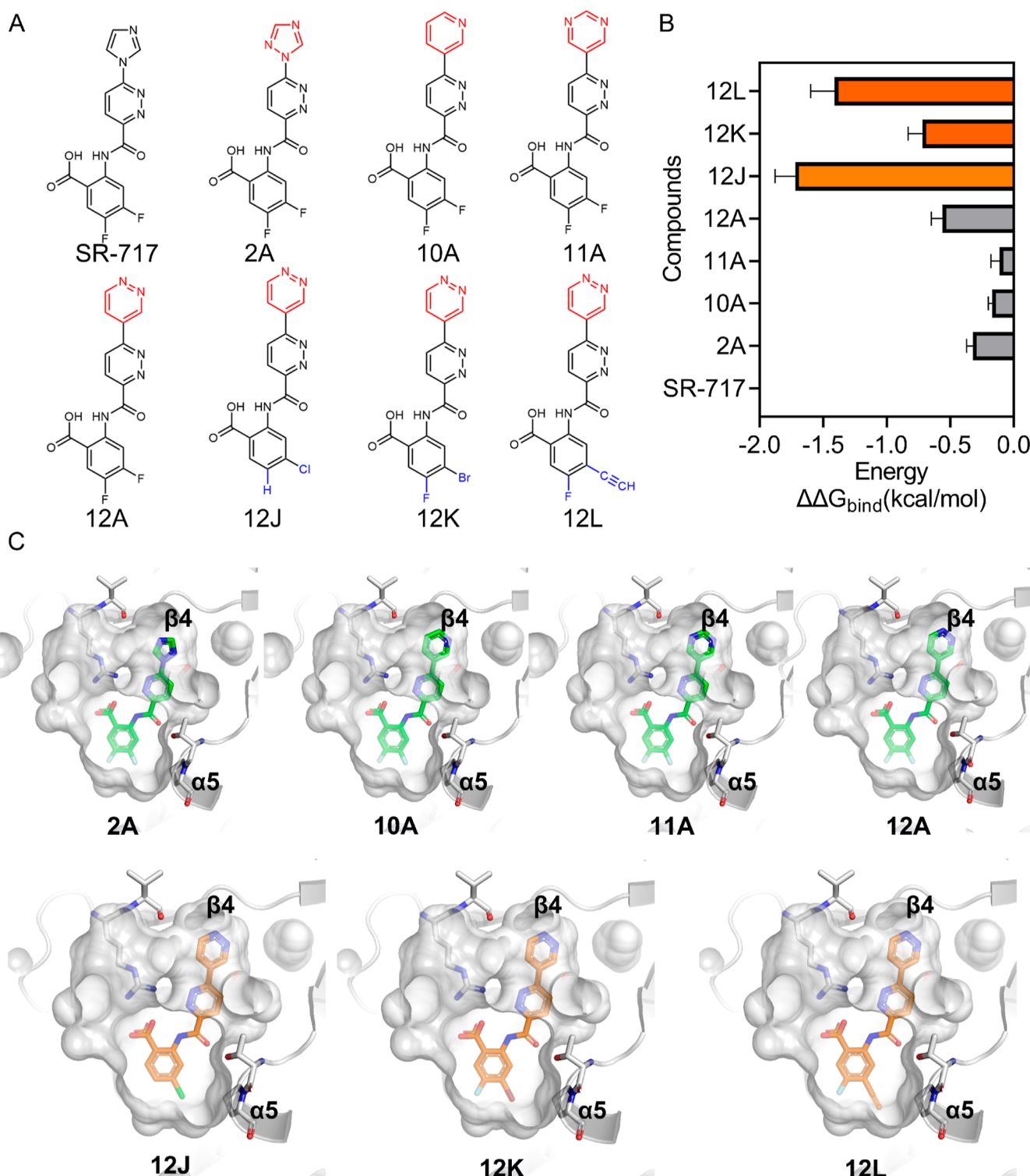


**Figure 7.** FEP calculations of STING agonists. (A) Chemical structures of eight STING agonists. (B) Relative binding free energies of STING agonists. (C) Binding modes of STING agonists. Key residues and agonists are depicted as sticks. The agonist-binding pocket is shown as the surface.

STING, the relative energies ( $\Delta\Delta G_{\text{bind}}$ ) of seven agonists were calculated (Figure 7, S9–S11 and Tables S4–S5). All of these agonists had a functional group different from the imidazole group of SR-717. In addition, a substitution of the fluorine of SR-717 yielded three compounds 12J, 12K, and 12L (Figure 7A). Among these compounds, 12J, 12K, and 12L had the lowest  $\Delta\Delta G_{\text{bind}}$  values of less than  $-0.6$  kcal/mol (Figure 7B).

and Table S5), suggesting that the substitution of the fluorine might influence agonist binding. In the previous competition binding assays, 12J, 12K, and 12L showed higher binding affinities with  $\text{IC}_{50}$  values of  $1.89$ ,  $1.75$ , and  $1.15 \mu\text{M}$ , compared with SR-717 ( $\text{IC}_{50} = 9.81 \mu\text{M}$ ),<sup>35</sup> highly consistent with our calculations. According to the binding models of these agonists to STING (Figure 7C),  $\beta 4$  and  $\alpha 5$  interacted with the

aromatic ring and the halogens (or alkynyl group), respectively. This demonstrates the importance of  $\beta 4$  and  $\alpha 5$  residues of STING in agonist binding. Additionally, in the THP1-cell system, the potency of 12J, 12K, and 12L ( $EC_{50}$  of 3.52, 2.78, and 0.38  $\mu M$ ) are stronger or comparable to those of SR-717 ( $EC_{50}$  of 3.03  $\mu M$ ).<sup>35</sup> These results again supported our calculations and highlighted the importance of the agonized-induced allosteric pathway involving  $\beta 4$  and  $\alpha 5$ . In particular,  $\alpha 5$  might play a crucial role in the activation of STING by all of these agonists. Targeting  $\alpha 5$  maybe a worth-trying strategy in developing potent STING agonists.

## CONCLUSIONS

For the importance target for treating cancer and immune disease, i.e., STING, we performed MD simulations to reveal the agonist-induced allosteric pathways for mediating STING and TBK1 interactions. Our MD simulations suggested that multiple helices ( $\alpha 5$ – $\alpha 7$ ) and especially three loops (loop 6, loop 8, and CTT) of STING are determinants in the allosteric activation of STING in the system including agonists as well as the constitutively activated mutant system. By employing the simulation models in the FEP calculation, we could further quantitatively characterize the structure–function relationships of multiple STING agonists, supported by the previous experimental data. Consequently, we find that helix  $\alpha 5$  is the key residue in the CBD pocket of STING during the TBK1 recruitment. Our work not only offers valuable insights into understanding the agonist-induced STING–TBK1 interactions but also paves the way for future agonist development of this important therapeutic target.

## METHODS

**Complex Modeling.** There is no experimental structure of human STING including both the C-terminal tail (CTT, residue IDs: 150–340) and the cyclic dinucleotide-binding domain (CBD, residue IDs: 340–379). But the crystal structure of the human TBK1 complex with the CTT of human STING (PDB code: 6O8B)<sup>33</sup> and the crystal structure of SR-717-bound CBD of human STING without CTT (PDB code: 6XNP)<sup>29</sup> are available. Thus, we used AlphaFold2<sup>36</sup> to construct models of human STING including CTT and CBD and employed available experimental structures as references for model selection. The amino acid sequence of human STING was obtained from the National Center for Biotechnology Information (379aa, Q8WV6.1)<sup>37</sup> and fed into AlphaFold2 to predict five different structure models of human STING. The predicted models were structurally aligned to the CTT binding to the TBK1 (PDB code: 6O8B) and the CBD binding to the SR-717 (PDB code: 6XNP), respectively (Figure S12). All models were verified with ERRAT and Ramachandran<sup>38</sup> (Table S6). The model with the minimum deviation from the experimental structure of STING was selected for the complex construction (Table S6). The  $C\alpha$  RMSD of CTT between the selected model and experimental structure (PDB code: 6O8B) was 0.94 Å, and the  $C\alpha$  RMSD between the model and experimental structure of STING (PDB code: 6XNP) was 0.67 Å. To construct the STING–TBK1 complex, we kept the TBK1 in the complex crystal structure (PDB code: 6O8B), and replaced the experimental structure of STING with the selected model including CTT and CBD. To construct the agonized-STING–TBK1 complex model, we structurally aligned the crystal structure of SR-717-

bound CBD (PDB code: 6O8B) to the STING–TBK1 complex model and then kept the SR-717 in the CBD of the STING–TBK1 complex model. To build the R284S–TBK1 complex, the R284 in the STING–TBK1 complex was mutated to a serine using PyMOL (Molecular Graphic System, Version 1.3, Schrodinger, LLC).

**System Preparation and Molecular Dynamics Simulation.** Simulation systems were prepared with Protein Preparation Wizard,<sup>39</sup> Prime module of Maestro from Schrodinger,<sup>40</sup> and AmberTools19.<sup>41,42</sup> The protonation states for the protein were chosen based on the results of PropKa calculation.<sup>43</sup> Protein parameters were assigned according to the ff14SB force field.<sup>44</sup> The antechamber bcc method<sup>45</sup> was used to optimize and charge the agonist molecule. The parameters of the general AMBER force field (GAFF)<sup>46</sup> were used. The protein complex was placed into a box of TIP3P water molecules<sup>47</sup> with a 0.5 nm buffer around the protein.  $Na^+$  and  $Cl^-$  salt ions were added at a 150 mM concentration. The periodic boundary conditions were applied to the simulation box (Table S7). For energy minimization (of 3000 steps), a set of steepest descents followed by conjugate gradient minimization were used. After energy minimization, 5000-step constant volume and temperature (NVT) and 50,000-step constant pressure and temperature (NPT) equilibrations were performed prior to production runs. During NVT equilibration, the volume and temperature (300 K) were controlled using the Berendsen thermostat.<sup>42</sup> During NPT equilibration, the temperature (300 K) and pressure (1 atm) were controlled using the default Berendsen with the isotropic position scaling method.<sup>43</sup> For production, a Langevin thermostat was used to control the temperature (300 K) and pressure (1 atm). In energy minimization, heavy atoms of solutes and crystal structure water were constrained with 2 kcal/mol/Å<sup>2</sup> using positional restraints. In NVT equilibration, heavy atoms of agonists and crystal structure water were constrained to 5 kcal/mol/Å<sup>2</sup> using positional restraints. No restraints were used in NPT equilibration and production. Equations of motion were integrated with a 2 fs time step. SHAKE algorithm was used to constrain bonds involving hydrogens. Nonbonded pair lists were generated every 10 steps using a distance cutoff of 1.4 nm. A cutoff of 1.2 nm was used for Lennard–Jones (excluding scales 1–4) interactions, which were smoothly switched off between 1 and 1.2 nm. Electrostatic interactions were computed using a particle-mesh Ewald algorithm<sup>48</sup> with a real-space cutoff of 1.2 nm. 1000 ns MD production run was performed for each complex system with independent replicates, using the PMEMD module.<sup>49</sup>

**Trajectory Analysis.** The “cluster” command in the AMBER cpptraj module was utilized to extract representative simulation models.<sup>50,51</sup> The clustering of each trajectory was performed by using the default hierarchical agglomerative (bottom-up) approach. Ten clusters were produced for each system with respect to the backbone atom RMSD of STING. We collected data from all replicates of a simulation system to calculate a particular measure. The last 200 ns trajectory of each replicate was selected for analysis. The cpptraj module was used to calculate the  $C\alpha$  RMSD and the heavy atom distances between residue pairs. The uncertainty of the distance represents the standard deviation of the mean. PISA was used to calculate the binding interface area of the protein complex.<sup>52</sup> DSSP was employed to analyze the variances of secondary structures in simulations, using the “secstruct”

module in AMBER cpptraj.<sup>53</sup> Dynamics cross-correlation matrices were calculated using the “matrix” command in AMBER cpptraj.<sup>53</sup>

**MMPBSA Calculations.** The MMPBSA models were calculated by MMPBSA.py. The single-trajectory MMPBSA protocol was used to analyze the agonist-STING complex interaction with the protein and agonist conformation in the bound and unbound states. The  $\Delta G_{\text{bind}}$  could be calculated in eq 1. Then, the binding free energy was decomposed as  $V_{\text{complex}}^{\text{vdW}}$ ,  $V_{\text{complex}}^{\text{ele}}$ ,  $\Delta G^{\text{polar}}$ , and  $\Delta G^{\text{nonpolar}}$  terms in eq 2.

$$\begin{aligned}\Delta G_{\text{bind,solv}} &= \Delta G_{\text{complex,solv}} + \Delta G_{\text{bind,vacuum}} \\ &\quad - (\Delta G_{\text{protein,solv}} + \Delta G_{\text{ligand,solv}})\end{aligned}\quad (1)$$

$$\Delta G_{\text{bind}} = V_{\text{complex}}^{\text{vdW}} + V_{\text{complex}}^{\text{ele}} + \Delta G^{\text{polar}} + \Delta G^{\text{nonpolar}} \quad (2)$$

**Free-Energy Perturbation Calculations.** The PyAutoFEP calculation protocol was used for relative binding free energy predictions of designed compounds.<sup>54</sup> The agonist SR-717 molecules were set as reference molecules. The OPLSAA force field was used during the FEP task. To obtain the binding free energy, a set of samples about conformations was collected by MD simulations at a bunch of lambda values between 0 and 1. The value of lambda was set as follows (VdwA: 1.00000 1.00000 1.00000 1.00000 1.00000 0.67479 0.45630 0.32525 0.24741 0.18978 0.11850 0.00000; VdwB: 0.00000 0.11850 0.18978 0.24741 0.32525 0.45630 0.67479 1.00000 1.00000 1.00000 1.00000 1.00000; coulA: 1.00000 0.75000 0.50000 0.25000 0.00000 0.00000 0.00000 0.00000 0.00000 0.00000 0.00000 0.00000; coulB: 0.00000 0.00000 0.00000 0.00000 0.00000 0.00000 0.00000 0.00000 0.00000 0.00000 0.00000 0.00000). Molecular dynamics was conducted for 5 ns per lambda.

## ASSOCIATED CONTENT

### Data Availability Statement

Molecular dynamics trajectories generated in this study are not publicly deposited as the data are over 16 GB in size. The data used to generate simulation results (input files, parameter files, topology files, etc.) are placed in the publicly available repository Zenodo (<https://zenodo.org/record/8098375>). Amber 18 software was used for MD simulations, and Gromacs 2021 was used for the FEP protocol.

### Supporting Information

The Supporting Information is available free of charge at <https://pubs.acs.org/doi/10.1021/acs.jcim.3c00984>.

#### SMILES data (TXT)

List of all reported average distances in different systems,  $C\alpha$  distance between N-terminal regions of  $\alpha 3$  helices in the published experimental structures of agonist-bound human STING, MMPBSA calculation of SR-717, FEP calculations of STING agonists, evaluation of AlphaFold2 predictions, simulation system information, multiple sequence alignment of STING,  $C\alpha$  distance of STING in the replicated simulations as a function of time, distributions of the  $C\alpha$  distances between  $\alpha 3$  and  $\alpha 3'$  of STING, distributions of the pairwise distance between key residues, time-course data showing the distance variances between key residues, helicity scores of three simulation models, DCCM analysis, key interactions in the mutation-induced activation of STING, energy

analysis of STING agonists, and construction of the STING–TBK1 complex model (PDF)

## AUTHOR INFORMATION

### Corresponding Authors

Hualiang Jiang – School of Pharmacy, China Pharmaceutical University, Nanjing 211198, China; State Key Laboratory of Drug Research, Shanghai Institute of Materia Medica, Chinese Academy of Sciences, Shanghai 201203, China; Email: [hlijiang@simm.ac.cn](mailto:hlijiang@simm.ac.cn)

Kaixian Chen – School of Pharmacy, China Pharmaceutical University, Nanjing 211198, China; State Key Laboratory of Drug Research, Shanghai Institute of Materia Medica, Chinese Academy of Sciences, Shanghai 201203, China; University of Chinese Academy of Sciences, Beijing 101408, China; Email: [kxchen@simm.ac.cn](mailto:kxchen@simm.ac.cn)

Xi Cheng – State Key Laboratory of Drug Research, Shanghai Institute of Materia Medica, Chinese Academy of Sciences, Shanghai 201203, China; University of Chinese Academy of Sciences, Beijing 101408, China; School of Pharmaceutical Science and Technology, Hangzhou Institute of Advanced Study, Hangzhou 310024, China;  [orcid.org/0000-0003-3735-645X](https://orcid.org/0000-0003-3735-645X); Email: [xicheng@simm.ac.cn](mailto:xicheng@simm.ac.cn)

### Authors

Rui Li – School of Pharmacy, China Pharmaceutical University, Nanjing 211198, China; State Key Laboratory of Drug Research, Shanghai Institute of Materia Medica, Chinese Academy of Sciences, Shanghai 201203, China

Lin Chen – State Key Laboratory of Drug Research, Shanghai Institute of Materia Medica, Chinese Academy of Sciences, Shanghai 201203, China

Xinheng He – State Key Laboratory of Drug Research, Shanghai Institute of Materia Medica, Chinese Academy of Sciences, Shanghai 201203, China; University of Chinese Academy of Sciences, Beijing 101408, China

Duanhua Cao – State Key Laboratory of Drug Research, Shanghai Institute of Materia Medica, Chinese Academy of Sciences, Shanghai 201203, China

Zehong Zhang – State Key Laboratory of Drug Research, Shanghai Institute of Materia Medica, Chinese Academy of Sciences, Shanghai 201203, China

Complete contact information is available at:  
<https://pubs.acs.org/10.1021/acs.jcim.3c00984>

### Author Contributions

R.L.: conceptualization, methodology, validation, formal analysis, investigation, data curation, writing—original draft, and visualization. L.C.: methodology and validation. X.H.: methodology and validation. D.C.: validation. Z.Z.: validation. H.J.: supervision and funding acquisition. K.C.: supervision and funding acquisition. X.C.: conceptualization, methodology, investigation, data curation, writing—review and editing, supervision, project administration, and funding acquisition.

### Notes

The authors declare no competing financial interest.

## ACKNOWLEDGMENTS

We would like to express our deepest gratitude to the late Professor Hualiang Jiang, who provided invaluable guidance and support for this project. This work was partially supported by the Shanghai Municipal Science and Technology Major

Project, Lingang Laboratory grant (LG202102-01-01), the Fund of Youth Innovation Promotion Association (2022077), and the National Key Research and Development Program of China (2021YFA1301900).

## ■ REFERENCES

- (1) Zheng, S.; Chang, W.; Liu, W.; Liang, G.; Xu, Y.; Lin, F. Computational Prediction of a New ADMET Endpoint for Small Molecules: Anticommensal Effect on Human Gut Microbiota. *J. Chem. Inf. Model.* **2019**, *59*, 1215–1220.
- (2) Amouzegar, A.; Chelvanambi, M.; Filderman, J. N.; Storkus, W. J.; Luke, J. J. STING Agonists as Cancer Therapeutics. *Cancers* **2021**, *13*, 2695.
- (3) Wolf, N. K.; Blaj, C.; Picton, L. K.; Snyder, G.; Zhang, L.; Nicolai, C. J.; Ndubaku, C. O.; McWhirter, S. M.; Garcia, K. C.; Raulet, D. H. Synergy of a STING agonist and an IL-2 superkine in cancer immunotherapy against MHC I-deficient and MHC I(+) tumors. *Proc. Natl. Acad. Sci. U.S.A.* **2022**, *119*, No. e2200568119.
- (4) Jing, W.; McAllister, D.; Vonderhaar, E. P.; Palen, K.; Riese, M. J.; Gershman, J.; Johnson, B. D.; Dwinell, M. B. STING agonist inflames the pancreatic cancer immune microenvironment and reduces tumor burden in mouse models. *J. Immunother. Cancer* **2019**, *7*, 115.
- (5) Kundu, N.; Kumar, A.; Corona, C.; Chen, Y.; Seth, S.; Karuppagounder, S. S.; Ratan, R. R. A STING agonist preconditions against ischaemic stroke via an adaptive antiviral Type 1 interferon response. *Brain Commun.* **2022**, *4*, fcac133.
- (6) Xu, N.; Palmer, D. C.; Robeson, A. C.; Shou, P.; Bommiasamy, H.; Laurie, S. J.; Willis, C.; Dotti, G.; Vincent, B. G.; Restifo, N. P.; Serody, J. S. STING agonist promotes CAR T cell trafficking and persistence in breast cancer. *J. Exp. Med.* **2021**, *218*, 218.
- (7) Zhang, H.; Han, M. J.; Tao, J.; Ye, Z. Y.; Du, X. X.; Deng, M. J.; Zhang, X. Y.; Li, L. F.; Jiang, Z. F.; Su, X. D. Rat and human STINGs profile similarly towards anticancer/antiviral compounds. *Sci. Rep.* **2015**, *5*, 18035.
- (8) Hinkle, J. T.; Patel, J.; Panicker, N.; Karuppagounder, S. S.; Biswas, D.; Belingon, B.; Chen, R.; Brahmachari, S.; Pletnikova, O.; Troncoso, J. C.; Dawson, V. L.; Dawson, T. M. STING mediates neurodegeneration and neuroinflammation in nigrostriatal alpha-synucleinopathy. *Proc. Natl. Acad. Sci. U.S.A.* **2022**, *119*, No. e2118819119.
- (9) Hong, C.; Schubert, M.; Tijhuis, A. E.; Requesens, M.; Roorda, M.; van den Brink, A.; Ruiz, L. A.; Bakker, P. L.; van der Sluis, T.; Pieters, W.; Chen, M.; Wardenaar, R.; van der Vegt, B.; Spiersings, D. C. J.; de Bruyn, M.; van Vugt, M.; Fojer, F. cGAS-STING drives the IL-6-dependent survival of chromosomally instable cancers. *Nature* **2022**, *607*, 366–373.
- (10) Li, S.; Mirlekar, B.; Johnson, B. M.; Brickey, W. J.; Wrobel, J. A.; Yang, N.; Song, D.; Entwistle, S.; Tan, X.; Deng, M.; Cui, Y.; Li, W.; Vincent, B. G.; Gale, M., Jr.; Pylayeva-Gupta, Y.; Ting, J. P. STING-induced regulatory B cells compromise NK function in cancer immunity. *Nature* **2022**, *610*, 373–380.
- (11) Liu, Y.; Xu, P.; Rivara, S.; Liu, C.; Ricci, J.; Ren, X.; Hurley, J. H.; Ablasser, A. Clathrin-associated AP-1 controls termination of STING signalling. *Nature* **2022**, *610*, 761–767.
- (12) Domizio, J. D.; Gulen, M. F.; Saidoune, F.; Thacker, V. V.; Yatim, A.; Sharma, K.; Nass, T.; Guenova, E.; Schaller, M.; Conrad, C.; Goepfert, C.; De Leval, L.; Garnier, C. v.; Berezowska, S.; Dubois, A.; Gilliet, M.; Ablasser, A. The cGAS-STING pathway drives type I IFN immunopathology in COVID-19. *Nature* **2022**, *603*, 145–151.
- (13) Jiang, M.; Chen, P.; Wang, L.; Li, W.; Chen, B.; Liu, Y.; Wang, H.; Zhao, S.; Ye, L.; He, Y.; Zhou, C. cGAS-STING, an important pathway in cancer immunotherapy. *J. Hematol. Oncol.* **2020**, *13*, 81.
- (14) Su, C. L.; Kao, Y. T.; Chang, C. C.; Chang, Y.; Ho, T. S.; Sun, H. S.; Lin, Y. L.; Lai, M. M. C.; Liu, Y. H.; Yu, C. Y. DNA-induced 2'3'-cGAMP enhances haplotype-specific human STING cleavage by dengue protease. *Proc. Natl. Acad. Sci. U.S.A.* **2020**, *117*, 15947–15954.
- (15) Eaglesham, J. B.; Pan, Y.; Kupper, T. S.; Kranzusch, P. J. Viral and metazoan poxins are cGAMP-specific nucleases that restrict cGAS-STING signalling. *Nature* **2019**, *566*, 259–263.
- (16) Zhou, Q.; Zhou, Y.; Li, T.; Ge, Z. Nanoparticle-Mediated STING Agonist Delivery for Enhanced Cancer Immunotherapy. *Macromol. Biosci.* **2021**, *21*, No. e2100133.
- (17) Messaoud-Nacer, Y.; Culquier, E.; Rose, S.; Maillet, I.; Rouxel, N.; Briault, S.; Ryffel, B.; Quesniaux, V. F. J.; Togbe, D. STING agonist diABZI induces PANoptosis and DNA mediated acute respiratory distress syndrome (ARDS). *Cell Death Dis.* **2022**, *13*, 269.
- (18) Pimkova Polidarova, M.; Brehova, P.; Dejmek, M.; Birkus, G.; Brazdova, A. STING Agonist-Mediated Cytokine Secretion Is Accompanied by Monocyte Apoptosis. *ACS Infect. Dis.* **2022**, *8*, 463–471.
- (19) Gao, P.; Ascano, M.; Zillinger, T.; Wang, W.; Dai, P.; Serganov, A. A.; Gaffney, B. L.; Shuman, S.; Jones, R. A.; Deng, L.; Hartmann, G.; Barchet, W.; Tuschl, T.; Patel, D. J. Structure-function analysis of STING activation by c[G(2',S')pA(3',S')p] and targeting by antiviral DMXAA. *Cell* **2013**, *154*, 748–762.
- (20) Aliakbar Tehrani, Z.; Rulisek, L.; Cerny, J. Molecular dynamics simulations provide structural insight into binding of cyclic dinucleotides to human STING protein. *J. Biomol. Struct. Dyn.* **2021**, *40* (20), 10250–10264.
- (21) Pimkova Polidarova, M.; Brehova, P.; Kaiser, M. M.; Smola, M.; Dracinsky, M.; Smith, J.; Marek, A.; Dejmek, M.; Sala, M.; Gutten, O.; Rulisek, L.; Novotna, B.; Brazdova, A.; Janeba, Z.; Nencka, R.; Boura, E.; Pav, O.; Birkus, G. Synthesis and Biological Evaluation of Phosphoester and Phosphorothioate Prodrugs of STING Agonist 3',3'-c-Di(2'F,2'dAMP). *J. Med. Chem.* **2021**, *64*, 7596–7616.
- (22) Xie, X.; Liu, J.; Wang, X. Design, Synthesis and Biological Evaluation of (2',S' and 3',S'-Linked) cGAMP Analogs that Activate Stimulator of Interferon Genes (STING). *Molecules* **2020**, *25* (22), S285.
- (23) Kempson, J.; Zhang, H.; Hou, X.; Cornelius, L.; Zhao, R.; Wang, B.; Hong, Z.; Oderinde, M. S.; Pawluczyk, J.; Wu, D. R.; Sun, D.; Li, P.; Yip, S.; Smith, A.; Caceres-Cortes, J.; Aulakh, D.; Sarjeant, A. A.; Park, P. K.; Harikrishnan, L. S.; Qin, L. Y.; Dodd, D. S.; Fink, B.; Vite, G.; Mathur, A. A Stereocontrolled Synthesis of a Phosphorothioate Cyclic Dinucleotide-Based STING Agonist. *J. Org. Chem.* **2021**, *86*, 8851–8861.
- (24) Basu, S.; Midya, S.; Banerjee, M.; Ghosh, R.; Pryde, D. C.; Yadav, D. B.; Shrivastava, R.; Surya, A. The discovery of potent small molecule cyclic urea activators of STING. *Eur. J. Med. Chem.* **2022**, *229*, 114087.
- (25) Gao, P.; Zillinger, T.; Wang, W.; Ascano, M.; Dai, P.; Hartmann, G.; Tuschl, T.; Deng, L.; Barchet, W.; Patel, D. J. Binding-pocket and lid-region substitutions render human STING sensitive to the species-specific drug DMXAA. *Cell Rep.* **2014**, *8*, 1668–1676.
- (26) Shih, A. Y.; Damm-Ganmet, K. L.; Mirzadegan, T. Dynamic Structural Differences between Human and Mouse STING Lead to Differing Sensitivity to DMXAA. *Biophys. J.* **2018**, *114*, 32–39.
- (27) Che, X.; Du, X. X.; Cai, X.; Zhang, J.; Xie, W. J.; Long, Z.; Ye, Z. Y.; Zhang, H.; Yang, L.; Su, X. D.; Gao, Y. Q. Single Mutations Reshape the Structural Correlation Network of the DMXAA-Human STING Complex. *J. Phys. Chem. B* **2017**, *121*, 2073–2082.
- (28) Pan, B. S.; Perera, S. A.; Piesvax, J. A.; Presland, J. P.; Schroeder, G. K.; Cumming, J. N.; Trotter, B. W.; Altman, M. D.; Buevich, A. V.; Cash, B.; Cemerski, S.; Chang, W.; Chen, Y.; Dandliker, P. J.; Feng, G.; Haidle, A.; Henderson, T.; Jewell, J.; Kariv, I.; Knemeyer, I.; Kopinja, J.; Lacey, B. M.; Laskey, J.; Lesburg, C. A.; Liang, R.; Long, B. J.; Lu, M.; Ma, Y.; Minnihan, E. C.; O'Donnell, G.; Otte, R.; Price, L.; Rakhilina, L.; Sauvagnat, B.; Sharma, S.; Tyagarajan, S.; Woo, H.; Wyss, D. F.; Xu, S.; Bennett, D. J.; Addona, G. H. An orally available non-nucleotide STING agonist with antitumor activity. *Science* **2020**, *369*, 369.
- (29) Chin, E. N.; Yu, C.; Vartabedian, V. F.; Jia, Y.; Kumar, M.; Gamo, A. M.; Vernier, W.; Ali, S. H.; Kissai, M.; Lazar, D. C.; Nguyen, N.; Pereira, L. E.; Benish, B.; Woods, A. K.; Joseph, S. B.; Chu, A.; Johnson, K. A.; Sander, P. N.; Martinez-Pena, F.; Hampton, E. N.;

- Young, T. S.; Wolan, D. W.; Chatterjee, A. K.; Schultz, P. G.; Petrossi, H. M.; Teijaro, J. R.; Lairson, L. L. Antitumor activity of a systemic STING-activating non-nucleotide cGAMP mimetic. *Science* **2020**, *369*, 993–999.
- (30) Ramanjulu, J. M.; Pesiridis, G. S.; Yang, J.; Concha, N.; Singhaus, R.; Zhang, S. Y.; Tran, J. L.; Moore, P.; Lehmann, S.; Eberl, H. C.; Muelbaier, M.; Schneck, J. L.; Clemens, J.; Adam, M.; Mehlmann, J.; Romano, J.; Morales, A.; Kang, J.; Leister, L.; Graybill, T. L.; Charnley, A. K.; Ye, G.; Nevins, N.; Behnia, K.; Wolf, A. I.; Kasparcova, V.; Nurse, K.; Wang, L.; Puhl, A. C.; Li, Y.; Klein, M.; Hopson, C. B.; Guss, J.; Bantscheff, M.; Bergamini, G.; Reilly, M. A.; Lian, Y.; Duffy, K. J.; Adams, J.; Foley, K. P.; Gough, P. J.; Marquis, R. W.; Smothers, J.; Hoos, A.; Bertin, J. Design of amidobenzimidazole STING receptor agonists with systemic activity. *Nature* **2018**, *564*, 439–443.
- (31) Kranzusch, P. J.; Wilson, S. C.; Lee, A. S.; Berger, J. M.; Doudna, J. A.; Vance, R. E. Ancient Origin of cGAS-STING Reveals Mechanism of Universal 2',3' cGAMP Signaling. *Mol. Cell* **2015**, *59*, 891–903.
- (32) Tsuchiya, Y.; Jounai, N.; Takeshita, F.; Ishii, K. J.; Mizuguchi, K. Ligand-induced Ordering of the C-terminal Tail Primes STING for Phosphorylation by TBK1. *EBioMedicine* **2016**, *9*, 87–96.
- (33) Zhao, B.; Du, F.; Xu, P.; Shu, C.; Sankaran, B.; Bell, S. L.; Liu, M.; Lei, Y.; Gao, X.; Fu, X.; Zhu, F.; Liu, Y.; Laganowsky, A.; Zheng, X.; Ji, J. Y.; West, A. P.; Watson, R. O.; Li, P. A conserved PLPLRT/SD motif of STING mediates the recruitment and activation of TBK1. *Nature* **2019**, *569*, 718–722.
- (34) King, E.; Aitchison, E.; Li, H.; Luo, R. Recent Developments in Free Energy Calculations for Drug Discovery. *Front. Mol. Biosci.* **2021**, *8*.
- (35) Shan, B.; Hou, H.; Zhang, K.; Li, R.; Shen, C.; Chen, Z.; Xu, P.; Cui, R.; Su, Z.; Zhang, C.; Yang, R.; Zhou, G.; Liu, Y.; Guo, H.; Chen, K.; Fu, W.; Jiang, H.; Zhang, S.; Zheng, M. Design, Synthesis, and Biological Evaluation of Bipyridazine Derivatives as Stimulator of Interferon Genes (STING) Receptor Agonists. *J. Med. Chem.* **2023**, *66*, 3327–3347.
- (36) Jumper, J.; Evans, R.; Pritzel, A.; Green, T.; Figurnov, M.; Ronneberger, O.; Tunyasuvunakool, K.; Bates, R.; Zidek, A.; Potapenko, A.; Bridgland, A.; Meyer, C.; Kohl, S. A. A.; Ballard, A. J.; Cowie, A.; Romera-Paredes, B.; Nikolov, S.; Jain, R.; Adler, J.; Back, T.; Petersen, S.; Reiman, D.; Clancy, E.; Zielinski, M.; Steinegger, M.; Pacholska, M.; Berghammer, T.; Bodenstein, S.; Silver, D.; Vinyals, O.; Senior, A. W.; Kavukcuoglu, K.; Kohli, P.; Hassabis, D. Highly accurate protein structure prediction with AlphaFold. *Nature* **2021**, *596*, 583–589.
- (37) Zhong, B.; Yang, Y.; Li, S.; Wang, Y. Y.; Li, Y.; Diao, F.; Lei, C.; He, X.; Zhang, L.; Tien, P.; Shu, H. B. The adaptor protein MITA links virus-sensing receptors to IRF3 transcription factor activation. *Immunity* **2008**, *29*, 538–550.
- (38) Laskowski, R. A.; Rullmann, J.; MacArthur, M. W.; Kaptein, R.; Thornton, J. M. AQUA and PROCHECK-NMR: programs for checking the quality of protein structures solved by NMR. *J. Biomol. NMR* **1996**, *8*, 477–486.
- (39) Madhavi Sastry, G.; Adzhigirey, M.; Day, T.; Annabhimmoju, R.; Sherman, W. Protein and ligand preparation: parameters, protocols, and influence on virtual screening enrichments. *J. Comput.-Aided Mol. Des.* **2013**, *27* (3), 221–234.
- (40) Jacobson, M. P.; Friesner, R. A.; Xiang, Z.; Honig, B. On the role of the crystal environment in determining protein side-chain conformations. *J. Mol. Biol.* **2002**, *320*, 597–608.
- (41) Salomon-Ferrer, R.; Case, D. A.; Walker, R. C. An overview of the Amber biomolecular simulation package. *Wiley Interdiscip. Rev.: Comput. Mol. Sci.* **2013**, *3*, 198–210.
- (42) Case, D. A.; Cheatham, T. E.; Darden, T.; Gohlke, H.; Luo, R.; Merz, K. M., Jr.; Onufriev, A.; Simmerling, C.; Wang, B.; Woods, R. J.; Woods, R. J. The Amber biomolecular simulation programs. *J. Comput. Chem.* **2005**, *26*, 1668–1688.
- (43) Olsson, M. H.; Sondergaard, C. R.; Rostkowski, M.; Jensen, J. H. PROPKA3: Consistent Treatment of Internal and Surface Residues in Empirical pKa Predictions. *J. Chem. Theory Comput.* **2011**, *7*, 525–537.
- (44) Maier, J. A.; Martinez, C.; Kasavajhala, K.; Wickstrom, L.; Hauser, K. E.; Simmerling, C. ff14SB: Improving the Accuracy of Protein Side Chain and Backbone Parameters from ff99SB. *J. Chem. Theory Comput.* **2015**, *11*, 3696–3713.
- (45) Jakalian, A.; Jack, D. B.; Bayly, C. I. Fast, efficient generation of high-quality atomic charges. AM1-BCC model: II. Parameterization and validation. *J. Comput. Chem.* **2002**, *23*, 1623–1641.
- (46) Wang, J.; Wolf, R. M.; Caldwell, J. W.; Kollman, P. A.; Case, D. A. Development and testing of a general amber force field. *J. Comput. Chem.* **2004**, *25*, 1157–1174.
- (47) de Souza, O. N.; Ornstein, R. L. Effect of warmup protocol and sampling time on convergence of molecular dynamics simulations of a DNA dodecamer using AMBER 4.1 and particle-mesh Ewald method. *J. Biomol. Struct. Dyn.* **1997**, *14* (5), 607–611.
- (48) Darden, T.; York, D.; Pedersen, L. Particle mesh Ewald: An N-log(N) method for Ewald sums in large systems. *J. Chem. Phys.* **1993**, *98*, 10089–10092.
- (49) Mermelstein, D. J.; Lin, C.; Nelson, G.; Kretsch, R.; McCammon, J. A.; Walker, R. C. Fast and flexible gpu accelerated binding free energy calculations within the amber molecular dynamics package. *J. Comput. Chem.* **2018**, *39*, 1354–1358.
- (50) Roe, D. R.; Cheatham, T. E., III PTTRAJ and CPPTRAJ: Software for Processing and Analysis of Molecular Dynamics Trajectory Data. *J. Chem. Theory Comput.* **2013**, *9*, 3084–3095.
- (51) Jörg Weiser, P. S. S.; Clark Still, W. Approximate Atomic Surfaces from Linear Combinations of Pairwise Overlaps (LCPO). *Journal of Chomput Chem.* **1998**, *20*, 217–230.
- (52) Schlee, S.; Straub, K.; Schwab, T.; Kinateder, T.; Merkl, R.; Sterner, R. Prediction of quaternary structure by analysis of hot spot residues in protein-protein interfaces: the case of anthranilate phosphoribosyltransferases. *Proteins* **2019**, *87*, 815–825.
- (53) Kabsch, W.; Sander, C. Dictionary of protein secondary structure: pattern recognition of hydrogen-bonded and geometrical features. *Biopolymers* **1983**, *22*, 2577–2637.
- (54) Carvalho Martins, L.; Cino, E. A.; Ferreira, R. S. PyAutoFEP: An Automated Free Energy Perturbation Workflow for GROMACS Integrating Enhanced Sampling Methods. *J. Chem. Theory Comput.* **2021**, *17*, 4262–4273.

## ■ NOTE ADDED AFTER ASAP PUBLICATION

The author name Kaixian Cheng was corrected to Kaixian Chen on October 17, 2023.